Hindawi Publishing Corporation
Journal of Nanomaterials
Volume 2015, Article ID 579489, 8 pages
http://dx.doi.org/10.1155/2015/579489

Research Article

Structural and Optical Properties of $CuInS_2$ Thin Films Prepared by Magnetron Sputtering and Sulfurization Heat Treatment

Rongfeng Guan,[1] Xiaoxue Wang,[2] and Qian Sun[1]

[1]*Laboratory for Advanced Technology in Environmental Protection of Jiangsu Province, Yancheng Institute of Technology, Yancheng, Jiangsu 224051, China*
[2]*School of Physics and Chemistry, Henan Polytechnic University, Jiaozuo, Henan 454000, China*

Correspondence should be addressed to Rongfeng Guan; rongfengg@163.com

Received 22 December 2014; Accepted 29 January 2015

Academic Editor: Wang Danping

Copyright © 2015 Rongfeng Guan et al. This is an open access article distributed under the Creative Commons Attribution License, which permits unrestricted use, distribution, and reproduction in any medium, provided the original work is properly cited.

$CuInS_2$ thin films were prepared by sulfurization of Cu-In precursor films through magnetron sputtering and the resulting films characterized using X-ray diffraction, Raman spectrometry, and UV-Vis spectrophotometry. The results demonstrate that a sputtering power of 80–120 W is more suitable for sputtered Cu-In precursor films and can be used to obtain $CuInS_2$ films with good crystallinity through vulcanization heat treatment. The sputtering gas pressure and sulfurization temperature were shown to impact on the film quality due to improper processes during the $CuInS_2$ phase. Some of the $CuIn_{11}S_{17}$ and CuS_2 impurities were observed in the composition of the prepared $CuInS_2$ thin films. Optimization of process parameters obtained from the experimental data was determined as a sputtering power of 80~120 W, a sputtering gas pressure of 0.6–0.8 Pa, a heat treatment temperature of 450~470°C, and a holding time of 2~3 hours. The optical band gap obtained for $CuInS_2$ thin films is between 1.48 and 1.5 eV.

1. Introduction

Copper indium disulfide ($CuInS_2$) is a ternary (I–III–VI) semiconductor with a direct band gap and a sulfide fullerene-like structure which belongs to groups II–VI replacing the copper and indium ions in group II. It has a chalcopyrite configuration with a phase transition temperature of 980°C. $CuInS_2$ has various advantages with a narrow band gap of 1.50 eV making it insensitive to temperature with good stability. It has high absorption coefficients, mostly at 10^5/cm, and can absorb 90% of sunlight for films of 1 to 2 μm thickness. All these advantages make $CuInS_2$ one of the most promising alternative absorbing semiconductor materials for the development of thin film solar cells [1–3].

$CuInS_2$ has anti-interference properties, a strong ability to resist radiation, a long service life, and lower toxic species compared to $CuInSe_2$. It has much potential as a thin film solar cell absorption material of the chalcopyrite semiconductors [4]. The theoretical efficiency for a $CuInS_2$ thin film solar cell is between 28 and 32% [5], but the highest conversion efficiency observed in the laboratory is only 13% [6, 7], which is significantly less than the predicted theoretical value. In the past few years, various methods of $CuInS_2$ synthesis have been reported including magnetron sputtering [8], spray pyrolysis [9, 10], ion layer gas reaction [11], chemical bath deposition [12], and electrodeposition [13–15]. For each of the above methods, magnetron sputtering has shown the most promise for the realization of thin film solar cells based on $CuInS_2$ for large-scale production. It is reported that Germany have established a thin film solar cell production line with battery conversion efficiency reaching 7.6% [16]. There are two main techniques of magnetron sputtering to obtain $CuInS_2$ thin film [17, 18]; one is the sputtering deposition of $CuInS_2$ thin film also containing the target Cu-In-S under the high vacuum. Under the same sputtering power and sputtering pressure, different elements of sputtering energy can be different, so it is therefore difficult to control the chemical composition. The other technique is sputtering Cu-In thin film with appropriate H_2S flow using a flow meter to control flow rate. The copper and indium atoms

Table 1: Different process parameters of samples synthesized by different sputtering power.

Sputtering power/W	Gas pressure/Pa	Target voltage/V	Target current/A	Deposition time/min	Treating temperature/°C	Holding time/h	Sulfur weight/g
80	0.4	566	0.14	20	500	2	1
100	0.4	531	0.19	20	500	2	1
120	0.4	573	0.21	20	500	2	1
140	0.4	560	0.25	20	500	2	1
160	0.4	570	0.28	20	500	2	1

continue to react with H_2S whilst sputtering on the substrate and finally forming a sulfide film. The difficulty associated with this method is the influence of the temperature and that H_2S is an inflammable, explosive, toxic gas which increases associated risks. In this paper, $CuInS_2$ thin films were prepared by sulfurization of Cu-In preformed films created by magnetron sputtering onto glass substrates. In the sulfurization process, solid sulfur powder was used as the sulfur source instead of H_2S. The effects of sputtering power, gas pressure, sulfurization temperature, and sulfurization time on the structural and optical properties of the $CuInS_2$ samples were determined.

2. Materials and Methods

2.1. Preparation of $CuInS_2$ Thin Film. The substrate was a high purity glass (99.99%) target with Cu-In alloy at a Cu/In atomic ratio of 1 : 1. This was in the size of Φ50 mm ∗ 4 mm. Argon was used as the sputtering gas with a distance of 8 cm between the target and substrate. First, the Cu-In precursor films were deposited on the substrate. The prepared precursor films were placed at high temperature in a tubular resistance furnace to prepare a $CuInS_2$ thin film by sulfurization heat treatment using argon gas as a protective gas to ventilate the tubular furnace.

2.2. Characterization. The crystalline phases of the samples were identified by laser confocal Raman spectroscopy system (Renishaw) and powder X-ray diffraction (XRD) measurements obtained using a D8 ADVANCE diffractometer with a Cu K_α radiation source ($\lambda = 0.15406$ nm). Data were collected over $2\theta = 5$–90°. The absorption spectra were investigated using a UV-Vis spectrometer (UV-2450) and the thickness of the films was investigated using a metallographic microscope (Olympus, ck40-M-F200) with image analyzer (Vms-2000).

3. Results and Discussion

3.1. The Influence of DC Sputtering Power on $CuInS_2$ Thin Films. The divided voltage of sputtering gas, the distance between target material and substrate, and the sputtering power were shown to be the influential factors on sputtering rate. Under the same conditions, with increasing sputtering power, the energy of incident ions was shown to increase. The deposition rate concerns the energy, quality, and incidence direction of the incident ions. Therefore, sputtering power

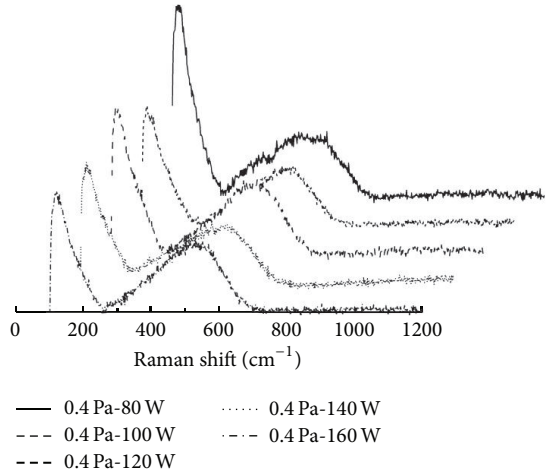

Figure 1: Raman spectra of the Cu-In thin films with different sputtering power before sulfuration.

is the main influential factor in controlling the deposition rate. In order to optimize the sputtering power, a working pressure of 0.4 Pa, and argon gas flow of 11 SCCM (standard mL/min), changes in sputtering power of 80, 100, 120, 140, and 160 W were observed. Table 1 shows the process parameters of coating and heat treatment.

Figure 1 shows the Raman spectra of Cu-In precursor films deposited at different sputtering powers. From the figure, it can be seen that the Raman spectra of Cu-In films have similar shapes, with wide spectra with wave numbers ranging from 230 cm^{-1} to 700 cm^{-1}. The results show low crystallinity as the Raman spectra are generated by molecular vibrations and atomic and interatomic forces acting on the alloy film. Consequently, some peaks are wide and the crystallinity is low. Cu-In films are required to react with sublimed sulfur during heat treatment making the sulfur be embedded into the films to form new phases and allow the crystals to regrow.

Figure 2 shows the Raman spectra of $CuInS_2$ thin films during sulfurization. Compared with Figure 1, new peaks with wave numbers in the range of 250~400 cm^{-1} are evident. For a sputtering power of 80 W, the Raman peak located at 298 cm^{-1} is consistent with the $CuInS_2$ chalcopyrite phase. When the sputtering powers are set to 100 and 120 W, corresponding Raman peaks occur at 313 cm^{-1} and 313 cm^{-1}. When the sputtering power is changed to 140 and 160 W,

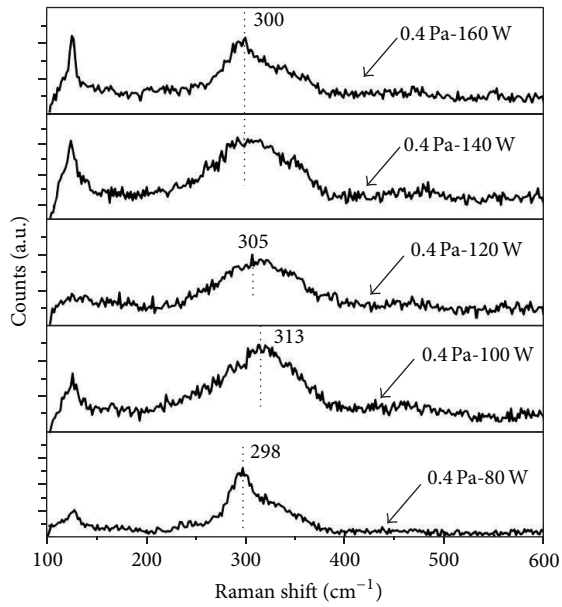

Figure 2: Raman spectra of the $CuInS_2$ thin films with different sputtering power.

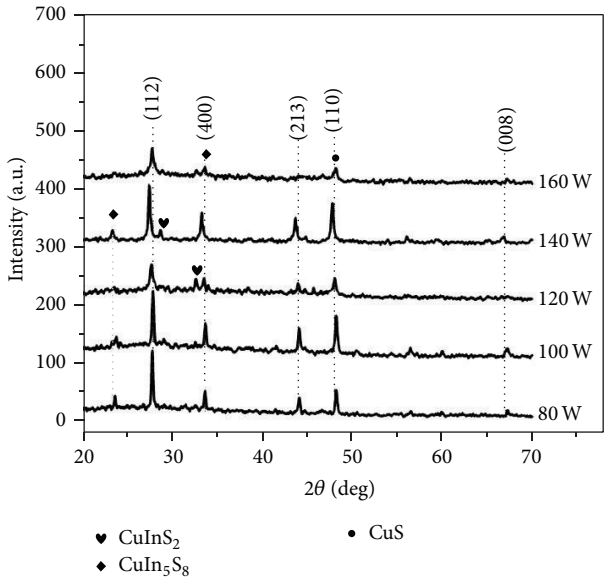

Figure 3: XRD spectra of the $CuInS_2$ thin films with different sputtering power (80 W, 100 W, 120 W, 140 W, and 160 W).

the Raman peaks are both located at 300 cm^{-1}, with a large FWHM (Full Width at Half Maximum) indicating more impurity in the phases and lower crystallinity compared with chalcopyrite $CuInS_2$.

Figure 3 shows the XRD spectra of the $CuInS_2$ thin films with different sputtering power (specifically 80, 100, 120, 140, and 160 W). The peaks in the XRD patterns for the samples are well matched with $CuInS_2$ (JCPDS number 65-1572), $CuIn_5S_8$ (JCPDS number 54-0554), and CuS (JCPDS number 65-3928). At sputtering powers of 80, 100, and 120 W, the $2\theta = 27.8^\circ$, 44°, and 67.3° are consistent with 112, 213, and 008 of $CuInS_2$ in the indices of lattice planes. For a sputtering power of 140 W, $2\theta = 28.9^\circ$, 44°, and 67.3° are consistent with 103, 213, and 008 of $CuInS_2$ in the indices of lattice planes. At a sputtering power of 160 W, $2\theta = 27.8^\circ$, 67.3° are consistent with 112 and 008 of $CuInS_2$ in the indices of lattice planes.

In addition to the characteristic diffraction peak of $CuInS_2$, the diffraction peaks of the CuS and $CuIn_5S_8$ phases are shown in Figure 3. All diffraction data were collected over $2\theta = 33.3^\circ$ with the crystal face index 400 consistent with the characteristic diffraction peak of $CuIn_5S_8$. Other diffraction data were collected over $2\theta = 48.2^\circ$ with the crystal face index 110 being consistent with the characteristic diffraction peak of CuS. There is not only the $CuInS_2$ phase but also CuS and $CuIn_5S_8$ phases that coexist in the film. This is due to Cu and S combining to form the CuS phase and In and S combining to form the In_2S_3 phase. CuS and In_2S_3 then further react on the surface of the thin film to form the CuS and $CuIn_5S_8$ phases. The diffraction spectra obtained at sputtering powers of 140 and 160 W have significant differences compared to the diffraction spectra of $CuInS_2$ (JCPDS number 65-1572). This may be due to the high sputtering power causing Cu and In to be accumulated too rapidly with uneven distribution of the elements. The formation of new phase disorders results in more lattice defects being produced when sulfur is embedded into the defective lattice and consequently generates the impurity phases. In conclusion, sputtering powers from 80 to 120 W are suitable to sputter the Cu-In precursor.

3.2. The Influence of Sputtering Gas Pressure on the Crystalline of Thin Films. As argon is used as the sputtering gas, the sputtering gas pressure is the partial pressure of argon in the vacuum chamber, the flow rate of which is controlled by a mass flow controller. The greater the argon flow rate value, the greater the sputtering gas pressure which is associated with the quality of thin films. The sputtering gas pressure ranges from 0.3 Pa to 0.8 Pa in the experiment. The process parameters of Cu-In preformed films were as follows: sputtering power was 80 W, the target voltage was 500 V, the target current was 0.16 A, and the argon gas flow was controlled at 11 SCCM, 16 SCCM, and 19 SCCM, which is consistent with the sputtering gas pressures of 0.4, 0.6, and 0.8 Pa in the coating chamber. The heat treating parameters were as follows: sulfurization temperature was 450°C, holding time was 3 hours, and the mass of sulfur was 2 g.

Figure 4 shows the Raman spectra of the $CuInS_2$ thin films obtained at different sputtering gas pressures. The Raman peak located at 298 cm^{-1} is consistent with the typical $CuInS_2$ chalcopyrite structure. When the sputtering gas pressure was set to 0.4 Pa, a Raman peak of 301 cm^{-1} which is next to the right side of 298 cm^{-1} emerged illustrating that the thin films prepared with the sputtering power in 0.4 Pa are a solid mixture of chalcopyrite and Cu-Au phases as the Raman FWHM value of Cu-Au phase is in the range of 290 cm^{-1} to 305 cm^{-1}. Compared with the other two curves (obtained at 0.4, 0.6 Pa), the Raman peak of 0.8 Pa sample has the highest intensity, the lowest FWHM values, and least defective structure.

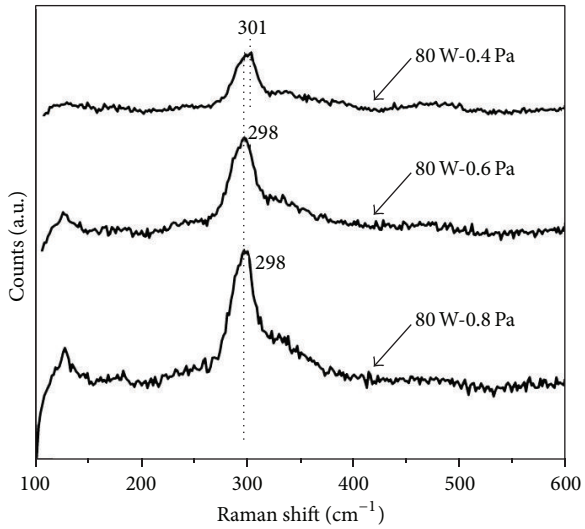

Figure 4: Raman spectra of the $CuInS_2$ thin films with different sputtering gas pressure (sputtering power of 80 W).

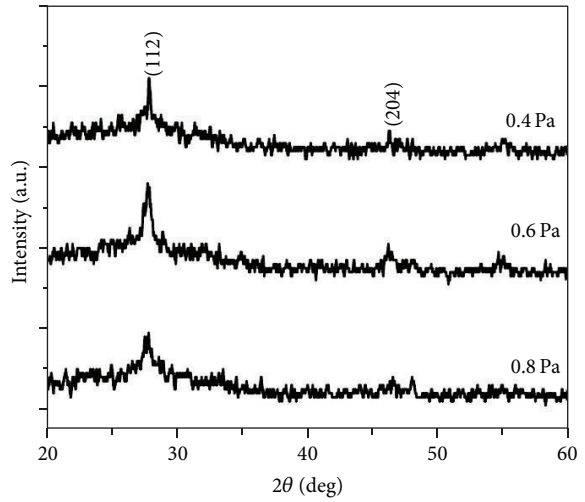

Figure 5: XRD spectra of the $CuInS_2$ thin films with different sputtering gas pressure (sputtering power of 80 W).

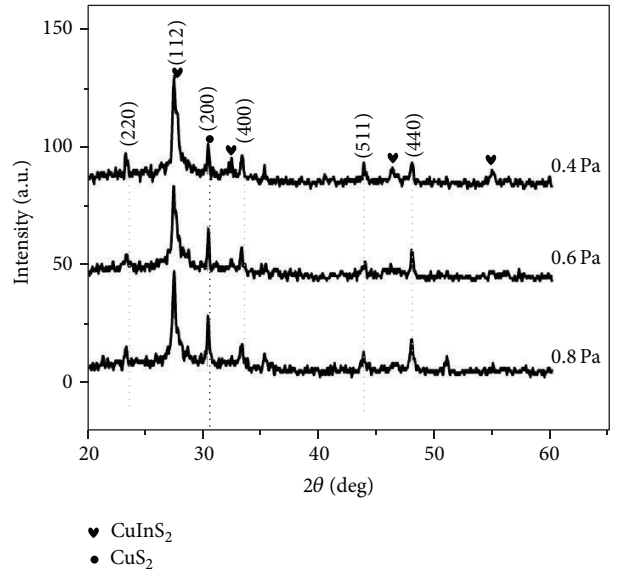

Figure 6: XRD spectra of the $CuInS_2$ thin films with different sputtering gas pressure (sputtering power of 110 W).

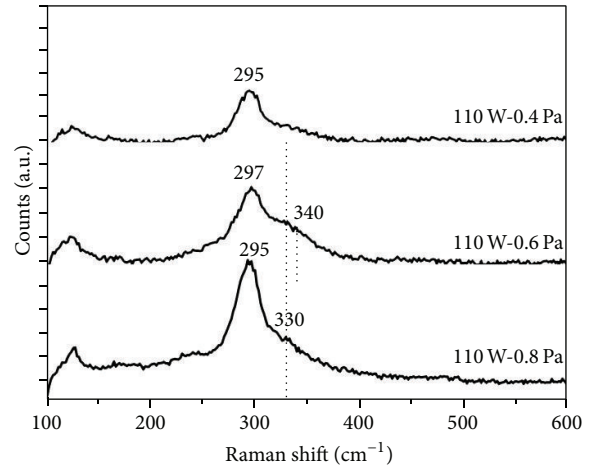

Figure 7: Raman spectra of the $CuInS_2$ thin films with different sputtering gas pressure (sputtering power of 110 W).

Figure 5 shows the XRD spectra for the vulcanized Cu-In thin films of different sputtering gas pressure. Compared with the $CuInS_2$ standard card (JCPSD number 65-1572), the intensity of peaks in the XRD pattern is low and the characteristic peaks located at $2\theta = 27.8^\circ$, 32.3°, and 46.3° are consistent with the crystal face indices 112, 004, and 204, respectively. The reason for the reduced diffraction intensity may be incomplete crystallization creating more impurity phases, resulting in more defective structures in the sulfurization process of the heat treatment.

In order to improve the crystallinity of the films, certain parameters were varied and the experiments repeated. The sputtering power was increased to 110 W; heat treatment temperature was increased to 470°C whilst keeping the other process parameters unchanged. These results are shown in Figures 6 and 7. Figure 6 shows the XRD spectra for the vulcanized Cu-In thin films of different sputtering pressures (specifically 0.4, 0.6, and 0.8 Pa). The information on the XRD patterns was obtained by comparing with the standard card $CuInS_2$ (JCPDS number 65-1572), $CuIn_{11}S_{17}$ (JCPDS number 34-0797), and CuS_2 (JCPDS number 65-4850). It can be seen from Figure 6 that the main diffraction peaks ($2\theta = 27.8^\circ$) can be attributed to $CuInS_2$. The thin films exhibit the preferred orientation along the 112 plane and better structure. For the 2θ of 32.3°, 43.8°, and 54.7°, each of these small diffraction peaks in the spectra is the characteristic peak of $CuInS_2$.

In addition, the other crystal face indices 220, 400, 511, and 440, which were marked in the spectra, are consistent with $2\theta = 23.5^\circ$, 33.4°, 43.8°, and 48°, respectively, and are attributed to $CuIn_{11}S_{17}$. For the $2\theta = 30.8^\circ$, this is attributed to CuS_2 with the crystal face index of 200. An

explanation of the form of the $CuIn_{11}S_{17}$ and CuS_2 phase is the uneven distribution of Cu and In in the thin films. Under the same conditions, the energy required to remove Cu and In out of the target material by sputtering is different and so different sputtering rates result in rich In being deposited on the substrate. Due to the small radius of the Cu atom and its disordered arrangement on the substrate, a part of it is embedded into In atoms. For the sulfurization process, the Cu and S atoms are naked on the surface of thin films and combine with nucleation to grow and form copper sulfides, such as CuS and CuS_2. Combined with S forms indium sulfides, copper sulfides then react with indium sulfides to form the $CuInS_2$ phase, where the Cu atoms are surrounded by In atoms that can combine with In and S atoms to form the new $CuIn_{11}S_{17}$ phase.

Figure 7 shows the Raman spectra of $CuInS_2$ thin films obtained in the second experiments. The Raman peaks located at 295 cm^{-1} and 297 cm^{-1} correspond to the structure of $CuInS_2$ chalcopyrite. When the sputtering pressure is at 0.6 Pa there is a less obvious Raman peak located at 340 cm^{-1}. According to the literature and XRD spectra, we can conclude that the peak is attributed to $CuIn_{11}S_{17}$ phase. With a sputtering pressure of 0.6 and 0.8 Pa, the intensity of the small Raman peak located at 330 cm^{-1} is low; according to the XRD spectra (Figure 6) it can be concluded that a CuS_2 phase is contained in the thin films. In contrast, when the sputtering pressure is at 0.6–0.8 Pa, the intensity of Raman peaks is higher and the FWHM value is lower with better crystallization and less phase impurity.

3.3. The Influence of Sulfurization Temperature on Crystallinity of the $CuInS_2$ Thin Films. The vulcanization heat treatment process is the key stage for Cu-In crystallization. Under the same conditions of sputtering power (110 W), the same sputtering pressure (0.6 Pa), and the same sputtering time of 20 minutes, sputtering batches of Cu-In prefabricated films were carried out using vulcanization heat treatment at temperatures of 450°C, 470°C, and 500°C. A holding time of 3 hours and sulfur amount of 2 g remained unchanged. The experimental results are shown in Figures 8 and 9.

Figure 8 shows the XRD spectra for Cu-In thin films of different temperatures. The diffraction peaks in the XRD patterns for the samples are well matched with the standard card of $CuInS_2$ (JCPDS number 65-1572), $CuIn_5S_8$ (JCPDS number 54-0554), and CuS (JCPDS number 65-4850), respectively. As shown, the main diffraction peaks (2θ = 27.8°) are attributed to $CuInS_2$. The thin films exhibited the preferred orientation along the 112 plane. The other diffraction peaks with the crystal face indices 220, 311, 400, 511, and 440 which were marked in the spectra are consistent with 2θ = 23.5°, 27.7°, 33.6°, 43.9°, and 48.1°, respectively; these are the characteristic peaks of $CuIn_5S_8$ and the 311 plane (2θ = 27.7°) overlapping with the 112 plane (2θ = 27.8°) of $CuInS_2$. In addition, diffraction peaks of the CuS_2 phase emerged in the XRD spectra at different temperatures corresponding to the 2θ = 30.8° and the crystal face index is 200. Compared with the other two spectra shown in Figure 8, when the heat treatment is 470°C, the crystallization of the $CuInS_2$ thin films is improved with less phase impurity.

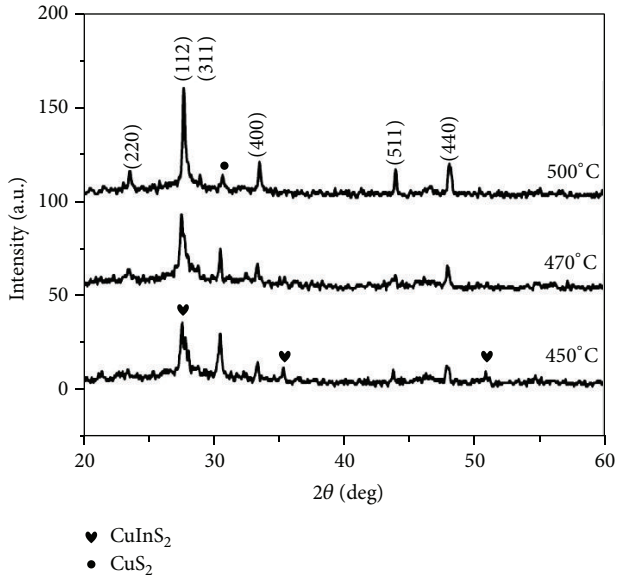

Figure 8: The XRD spectra of the $CuInS_2$ thin films with different sulfuration temperature.

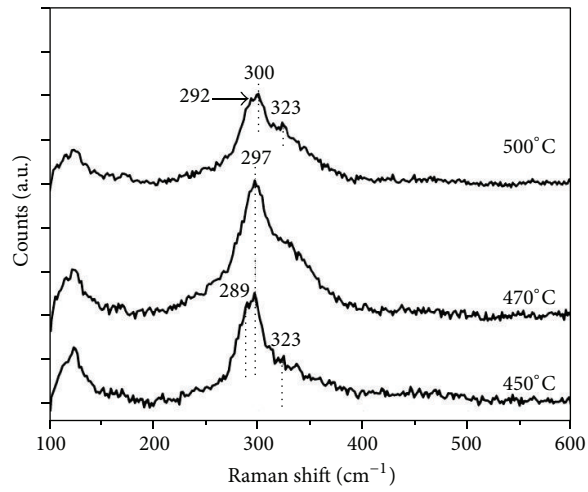

Figure 9: Raman spectra of the $CuInS_2$ thin films with different sulfuration temperature.

Figure 9 shows the Raman spectra of the thin films obtained at different sulfide heat treatment temperatures for three hours, the two main Raman peaks 289 cm^{-1} and 297 cm^{-1} corresponding to the $CuInS_2$ chalcopyrite phase, and another peak 323 cm^{-1} which corresponds to the β-In_2S_3 phase. At a sulfurization temperature of 470°C, the Raman peak located at 297 cm^{-1} corresponds to the symbionts of $CuInS_2$ chalcopyrite and Cu-Au phases. At the sulfurization temperature of 500°C, the two main Raman peaks located at 292 cm^{-1} and 300 cm^{-1} show that the structure is not a single chalcopyrite phase but the symbionts of the $CuInS_2$ chalcopyrite and Cu-Au phases. There is also a peak located at 323 cm^{-1} corresponding to the β-In_2S_3 phase, similar to that at 450°C. In contrast to the Raman peak of $CuInS_2$ thin film

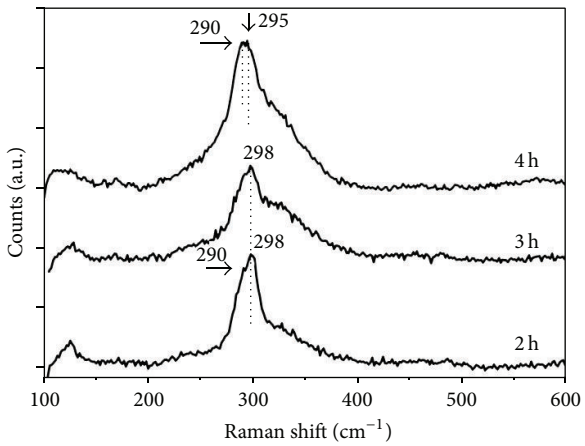

FIGURE 10: Raman spectra of the $CuInS_2$ thin films with different holding time.

of 470°C, the FWHM values are reduced, the chalcopyrite structure is unitary, and the crystallinity is improved.

3.4. The Influence of Heat Treatment Time on Crystallinity of the $CuInS_2$ Thin Films. The experimental results are shown in Figure 10 for sputtering out a batch of Cu-In prefabricated films and carrying on vulcanization heat treatment at different holding times of 2 hours, 3 hours, and 4 hours. Other parameters were at a sputtering power of 80 W, a sputtering gas pressure of 0.4 Pa, a sputtering time of 20 minutes, a sulfurization temperature of 500°C, and a sulfur amount of 2 g.

Figure 10 is the Raman spectra of the $CuInS_2$ thin films with different holding times. The two main Raman peaks at 290 cm^{-1} and 298 cm^{-1} correspond to holding times of 2 hours during the $CuInS_2$ chalcopyrite phase. At a holding time of 3 hours, a single main Raman peak is observed located at 298 cm^{-1}. At a holding time of 4 hours, there are two Raman peaks located at 290 cm^{-1} and 295 cm^{-1}, both of which are the characteristic peaks of chalcopyrite structure. Therefore, at a holding time of 2 hours, the intensity of the Raman peak is higher, the FWHM value is decreased, and the crystallinity is improved.

3.5. The Morphology and Optical Properties of $CuInS_2$ Thin Films. The optical band gap is calculated using the following equation: $\alpha h\nu = A(h\nu - E_g)^n$. In this equation, $h\nu$ is the photon energy, α is the absorption coefficient of the thin film, E_g is the optical band gap, and A is the bandwidth coefficient, which is connected with refractive index and the direct transition oscillator strength; it is a constant value and for the direct band gap semiconductor materials n is 1/2. According to this equation, the optical band gap of the thin films can be estimated.

Figure 11 shows the SEM micrographs of $CuInS_2$ thin films synthesized under the optimized process conditions (the holding time of 2 hours; the sulfurization temperature of 470°C; a sputtering pressure of 0.8 Pa; a sputtering power of 80 W). The micrographs shown in Figure 11(a) suggest that

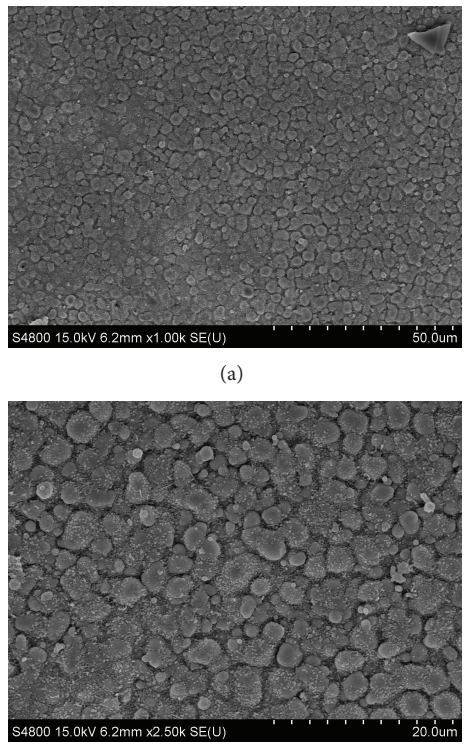

FIGURE 11: SEM micrographs of the samples prepared under the optimized condition: the holding time is 2 h; the sulfurization temperature is 470°C; the sputtering pressure is 0.8 Pa; the sputtering power is 80 W.

the grains are relatively evenly distributed and consist mostly of grains around 2–5 μm. This data also shows that the grains are spherical; however, Figure 11(b) suggests that the spherical grains are deposited by many small particles. It is known that smaller, nanosized particles can easily and spontaneously agglomerate to form larger particles.

Figure 12 shows the optical band gap of $CuInS_2$ thin films at process parameters indicated. The optical band gap values of the $CuInS_2$ thin films are 1.48 eV and 1.5 eV, respectively. In addition, metallographic microscope and metallographic image analysis were applied to measure the thickness of the thin films, with the average thickness ranging from 4 to 7 μm.

4. Conclusions

Using magnetron sputtering and sulfurization heat processes is an effective method to prepare $CuInS_2$ thin film. The sputtering pressure and sulfurization temperatures have a large influence on the quality of thin films. When improperly choosing process parameters, these will affect not only the $CuInS_2$ phase but also the $CuIn_{11}S_{17}$ and CuS_2 phases. The optical band gaps of prepared $CuInS_2$ thin film are around 1.48–1.5 eV. Based on the experiment results, the optimized process parameters are as follows: a sputtering power ranging from 80 to 120 W, a sputtering pressure of 0.6–0.8 Pa with the heat treatment temperature in the range of 450 to 470°C, and

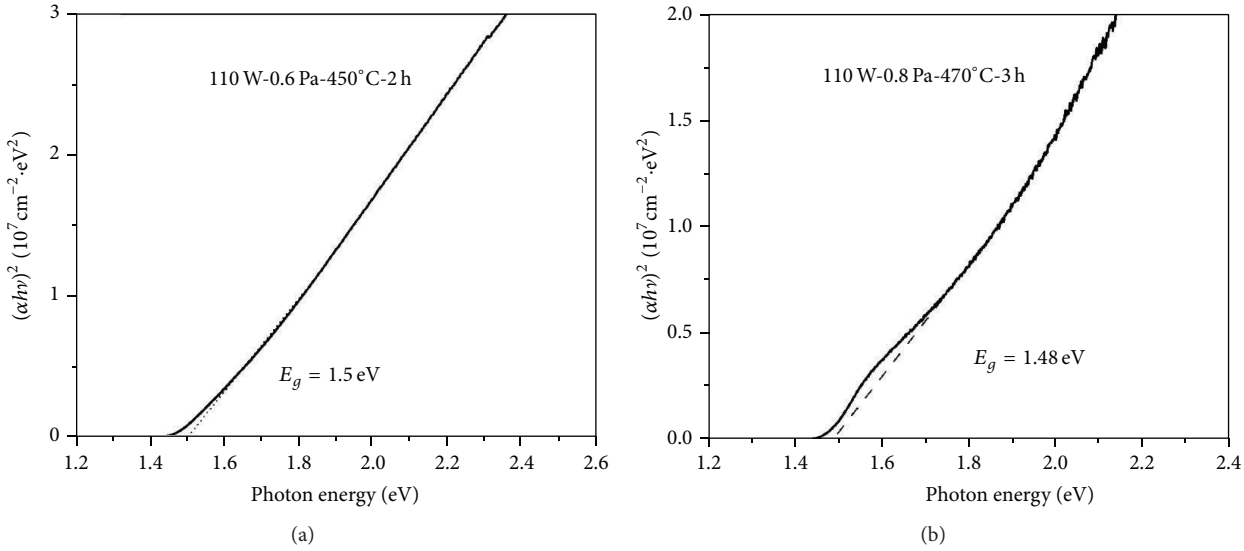

Figure 12: The optical band gap of $CuInS_2$ thin films synthetized by different sulfuration conditions.

a holding time ranging from 2 to 3 hours. The thickness of the $CuInS_2$ thin film is between 6 and 10 μm.

Conflict of Interests

The authors declare that there is no conflict of interests regarding the publication of this paper.

Acknowledgments

This work was financially supported by the National Natural Science Foundation (no. 21276220), National Key Technology Support Program (no. 2013BAC13B00), and Yancheng Institute of Technology Talent Program (no. KJC2013007).

References

[1] W. Yao, Y. Wang, X. Wang, J. Zhu, Z. Zhang, and X. Yuan, "$CuInS_2$ thin films obtained by solid-state sulfurization," *Materials Science in Semiconductor Processing*, vol. 26, no. 1, pp. 175–181, 2014.

[2] Z. Peng, Y. Liu, Y. Zhao et al., "ZnSe passivation layer for the efficiency enhancement of $CuInS_2$ quantum dots sensitized solar cells," *Journal of Alloys and Compounds*, vol. 587, pp. 613–617, 2014.

[3] T. Li, X. Li, Q. Zhao, Y. Shi, and W. Teng, "Fabrication of n-type $CuInS_2$ modified TiO_2 nanotube arrays heterostructure photoelectrode with enhanced photoelectrocatalytic properties," *Applied Catalysis B: Environmental*, vol. 156-157, pp. 362–370, 2014.

[4] K. Siemer, J. Klaer, I. Luck, J. Bruns, R. Klenk, and D. Bräunig, "Efficient $CuInS_2$ solar cells from a rapid thermal process (RTP)," *Solar Energy Materials and Solar Cells*, vol. 67, no. 1–4, pp. 159–166, 2001.

[5] J. J. M. Binsma, L. J. Giling, and J. Bloem, "Luminescence of $CuInS_2$. I. The broad band emission and its dependence on the defect chemistry," *Journal of Luminescence*, vol. 27, no. 1, pp. 35–53, 1982.

[6] H. Goto, Y. Hashimoto, and K. Ito, "Efficient thin film solar cell consisting of TCO/CdS/$CuInS_2$/$CuGaS_2$ structure," *Thin Solid Films*, vol. 451-452, pp. 552–555, 2004.

[7] T. Nakabayashi, T. Miyazawa, Y. Hashimoto, and K. Ito, "Over 10% efficient CuInS2 solar cell by sulfurization," *Solar Energy Materials & Solar Cells*, vol. 49, no. 1–4, pp. 375–381, 1997.

[8] S. Seeger and K. Ellmer, "Reactive magnetron sputtering of $CuInS_2$ absorbers for thin film solar cells: problems and prospects," *Thin Solid Films*, vol. 517, no. 10, pp. 3143–3147, 2009.

[9] A. S. Cherian, K. B. Jinesh, Y. Kashiwaba et al., "Double layer $CuInS_2$ absorber using spray pyrolysis: a better candidate for $CuInS_2$/In_2S_3 thin film solar cells," *Solar Energy*, vol. 86, no. 6, pp. 1872–1879, 2012.

[10] D.-Y. Lee and J. Kim, "Deposition of $CuInS_2$ films by electrostatic field assisted ultrasonic spray pyrolysis," *Solar Energy Materials and Solar Cells*, vol. 95, no. 1, pp. 245–249, 2011.

[11] C.-H. Fischer, N. A. Allsop, S. E. Gledhill et al., "The spray-ILGAR (ion layer gas reaction) method for the deposition of thin semiconductor layers: process and applications for thin film solar cells," *Solar Energy Materials & Solar Cells*, vol. 95, no. 6, pp. 1518–1526, 2011.

[12] G.-T. Pan, M.-H. Lai, R.-C. Juang, T.-W. Chung, and T. C.-K. Yang, "The preparation and characterization of Ga-doped $CuInS_2$ films with chemical bath deposition," *Solar Energy Materials & Solar Cells*, vol. 94, no. 10, pp. 1790–1796, 2010.

[13] S. M. Lee, S. Ikeda, Y. Otsuka, W. Septina, T. Harada, and M. Matsumura, "Homogeneous electrochemical deposition of in on a Cu-covered Mo substrate for fabrication of efficient solar cells with a $CuInS_2$ photoabsorber," *Electrochimica Acta*, vol. 79, pp. 189–196, 2012.

[14] S. Ebrahim, I. Morsi, M. Soliman, M. Elsharkawi, and A. Elzaem, "Preparation and characterization of chalcopyrite compound for thin film solar cells," *Alexandria Engineering Journal*, vol. 50, no. 1, pp. 35–42, 2011.

[15] C. Broussillou, M. Andrieux, M. Herbst-Ghysel et al., "Sulfurization of Cu–In electrodeposited precursors for $CuInS_2$-based

solar cells," *Solar Energy Materials & Solar Cells*, vol. 95, no. 1, pp. S13–S17, 2011.

[16] N. Meyer, A. Meeder, and D. Schmid, "Pilot production of large-area $CuInS_2$-based solar modules," *Thin Solid Films*, vol. 515, no. 15, pp. 5979–5984, 2007.

[17] Y. B. He, A. Krost, J. Bläsing et al., "Quasi-epitaxial growth of thick $CuInS_2$ films by RF reactive sputtering with a thin epilayer buffer," *Thin Solid Films*, vol. 451-452, pp. 229–232, 2004.

[18] Y. B. He, W. Kriegseis, T. Krämer et al., "Deposition of $CuInS_2$ thin films by RF reactive sputtering with a ZnO:Al buffer layer," *Journal of Physics and Chemistry of Solids*, vol. 64, no. 9-10, pp. 2075–2079, 2003.

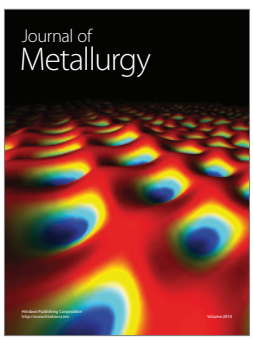

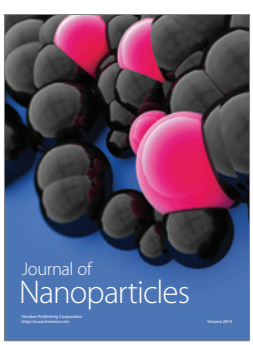

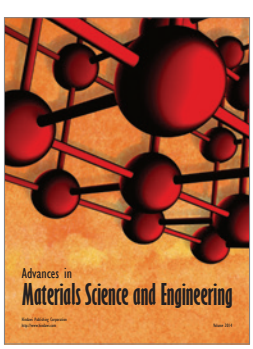

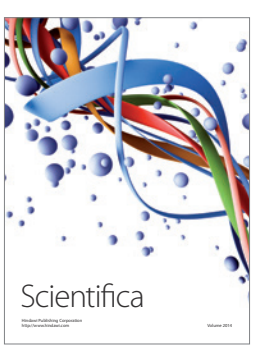

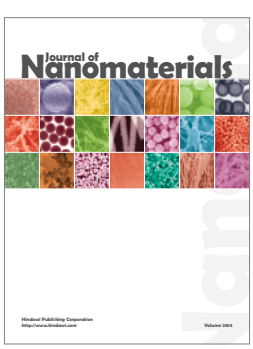

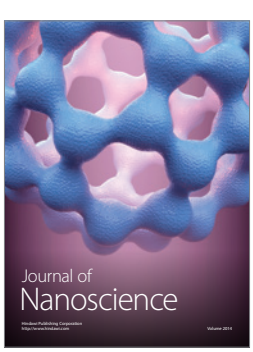

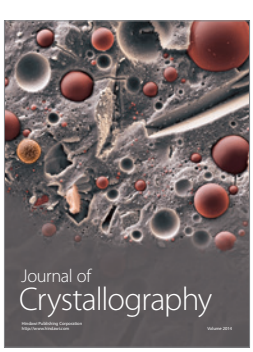

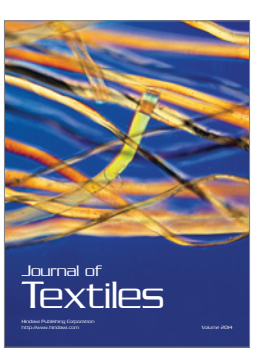

Hindawi

Submit your manuscripts at
http://www.hindawi.com